Parametric design and optimization of a shredder rotor carriage using ANSYS Workbench

E K Tesema[1,*], H G Lemu[2] and F T Daba[3]

[1]Technion – Israel Institute of Technology, Faculty of Civil and Environmental Engineering, Technion City, Haifa 3200003, Israel
[2]University of Stavanger, Faculty of Science and Technology, Stavanger, Norway
[3]Addis Ababa Science and Technology University (AASTU), Addis Ababa, Ethiopia

E-mail: edosa.tesema@campus.technion.ac.il

Abstract. This study investigates the response-surface-based parametric optimization of a plastic-shredder rotor blade carriage using SolidWorks and ANSYS Workbench. Five geometric dimensions were considered using a 27-point central composite design and response-surface optimization. The geometric design space was defined using parameter-specific bounds. Static finite element analysis provided maximum deformation, maximum von Mises stress, and minimum factor of safety. Response surfaces were constructed using the Genetic Aggregation method, and a multi-objective genetic algorithm was employed to identify candidate designs. Of the three reported candidates, Candidate 3 was selected for dimensional reconstruction. Relative to the original finite element results, its unrounded surrogate predictions indicate an 11.12% reduction in deformation, a 7.83% reduction in equivalent stress, and a 10.06% increase in minimum factor of safety. The reported improvements are surrogate-based predictions rather than direct finite element results for the reconstructed final geometry.

Keywords: Plastic shredder blade carriage, Parametric optimization, Finite element analysis, Central composite design, Response surface, Multi-objective genetic algorithm

1 Introduction

Mechanical recycling is an established route for recovering thermoplastic waste, in which size reduction is required before subsequent cleaning, separation, and reprocessing operations [1], [2]. Plastic shredders perform this function by reducing waste into smaller fragments suitable for further processing. Their performance depends strongly on the configuration and geometry of the shaft, rotor, cutting blades, and supporting components [3]. During shredding, these components are subjected to considerable mechanical loads; therefore, their design must provide sufficient stiffness, strength, and structural safety while remaining manufacturable.

Structural optimization provides a systematic means of improving mechanical components by modifying material distribution or geometric parameters to satisfy prescribed performance requirements. Common approaches include topology, size, shape, and parametric optimization [4]. Topology optimization identifies an efficient material distribution within a prescribed design domain, whereas parametric optimization refines an existing geometry by varying selected dimensions while preserving its basic topology. Parametric optimization is therefore particularly suitable for detailed design, where dimensions such as thicknesses, radii, and feature locations must be adjusted within practical limits. The integration of topology and shape optimization

can further support the transition from an optimized conceptual layout to a manufacturable CAD geometry [5].

Efficient parametric optimization requires close integration between computer-aided design (CAD), finite element analysis (FEA), and numerical optimization. Park and Dang [6] demonstrated that CAD–CAE integration combined with metamodeling can automate the design–analysis–redesign cycle and reduce the computational effort required for structural optimization. Because direct evaluation of every possible combination of design variables is generally impractical, surrogate models can be used to approximate the relationships between geometric parameters and structural responses using a limited number of simulations [7].

Design of Experiments (DOE) and Response Surface Methodology (RSM) provide an efficient framework for exploring multidimensional design spaces. The response-surface concept introduced by Box and Wilson [8] forms the basis for approximating relationships between controllable variables and system responses, while DOE provides a systematic procedure for generating representative combinations of design variables [9]. In structural optimization, these methods can relate geometric parameters to responses such as deformation, equivalent stress, and factor of safety. Sensitivity analysis can then identify the parameters with the greatest influence on structural performance and guide optimization toward effective regions of the design space.

Optimization-based design has been successfully applied to a wide range of engineering structures. Cavazzuti et al. [10] applied topology-based optimization to the development of a lightweight automotive chassis, while Li et al. [11] combined topology, shape, and size optimization in the design of an automotive engine cradle. Zhu et al. [12] reported extensive applications of topology optimization in aircraft and aerospace structures. Parametric and topology-based optimization has also been applied to mechanical components, demonstrating the effectiveness of parameter-driven design for improving structural performance while satisfying geometric constraints [13].

Similar optimization approaches have increasingly been applied to plastic shredder components. Trad et al. [14] combined FEA, DOE, and RSM to optimize a plastic shredder rotor and reported reductions in stress and deformation. Tesema and Lemu [15] applied topology optimization to a plastic-shredding-machine blade carriage and achieved a 17.5% reduction in mass while maintaining an acceptable factor of safety. Nguyen et al. [16] investigated the geometric optimization of a plastic bottle shredder blade using numerical analysis and RSM. These studies demonstrate that the structural performance of shredder components can be improved through numerical optimization.

Topology optimization establishes an efficient material layout, but the reconstructed geometry still contains dimensional features whose values can significantly influence deformation, stress, and structural safety. A systematic parametric study is therefore required to determine an improved combination of these dimensions rather than relying on repeated trial-and-error modifications. The specific contribution of the present work is to refine a previously topology-optimized, detachable splined blade carriage through a five-variable DOE, response-surface-based sensitivity analysis, and multi-objective dimensional optimization, rather than to develop a new shredder topology or a new optimization algorithm. Accordingly, the present study investigates the parametric design and optimization of a plastic-shredder rotor blade carriage using SolidWorks and ANSYS Workbench. The geometry is based on a previously topology-optimized blade carriage [15] and is further refined through dimensional parameterization. Five geometric dimensions are defined as input variables, while maximum total deformation, maximum equivalent stress, and minimum factor of safety are considered as structural responses. A DOE consisting of 27 design points was generated, followed by response-surface modelling, local and

global sensitivity analyses, and multi-objective optimization. The final candidate was selected from the predicted response trade-offs and reconstructed with nominal CAD dimensions.

2 Methodology

This study combined computer-aided design (CAD), finite element analysis (FEA), and response-surface-based parametric optimization to investigate the structural performance of a single-shaft plastic shredder rotor blade carriage. The carriage geometry was derived from a previously topology-optimized design [15]. SolidWorks was employed for geometric modeling and parameterization, while ANSYS Workbench was used for static structural analysis, design of experiments, response-surface analysis, sensitivity assessment, and multi-objective optimization. Figure 1 summarizes the study workflow.

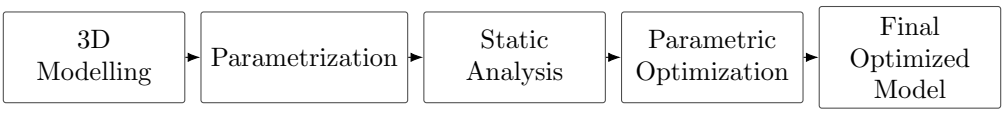


Figure 1: Workflow of the study.

2.1 Geometric Modeling and Finite Element Analysis

Three shaft–carriage attachment arrangements were initially investigated: cylindrical, hexagonal, and splined configurations (Figure 2). For this preliminary comparison, a single blade carriage was mounted on a full-length shaft to represent each connection arrangement. The cylindrical configuration included a welded connection, whereas the hexagonal and splined arrangements used matching noncircular shaft–hub profiles. The objective of this comparison was to select an appropriate attachment arrangement under consistent numerical conditions, rather than to optimize the geometric dimensions.

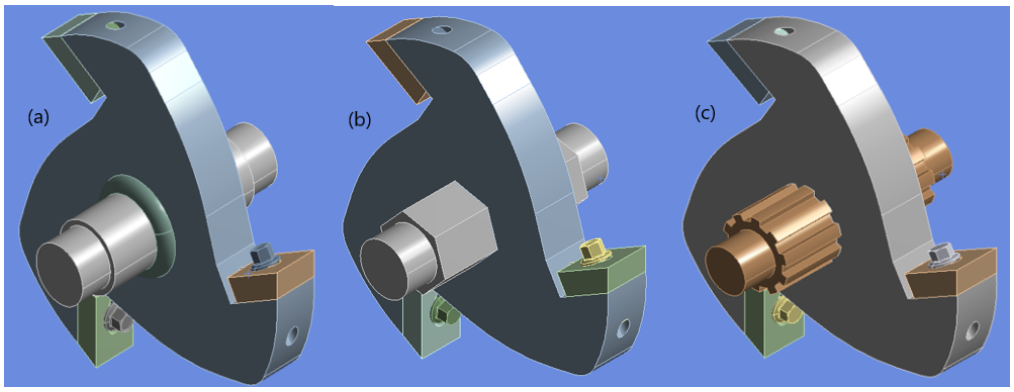


Figure 2: Shaft–carriage attachment mechanisms: (a) cylindrical, (b) hexagonal, and (c) splined.

The preliminary static structural models were assigned structural steel. Rough contact was specified at the shaft–carriage interface and bonded contact at the other applicable interfaces, as described in the original comparative analysis. Automatic meshing in ANSYS Mechanical was used with tetrahedral elements, a nominal element size of 5 mm, and a fine span-angle-center setting. This element size was used only for the preliminary shaft–carriage comparison;

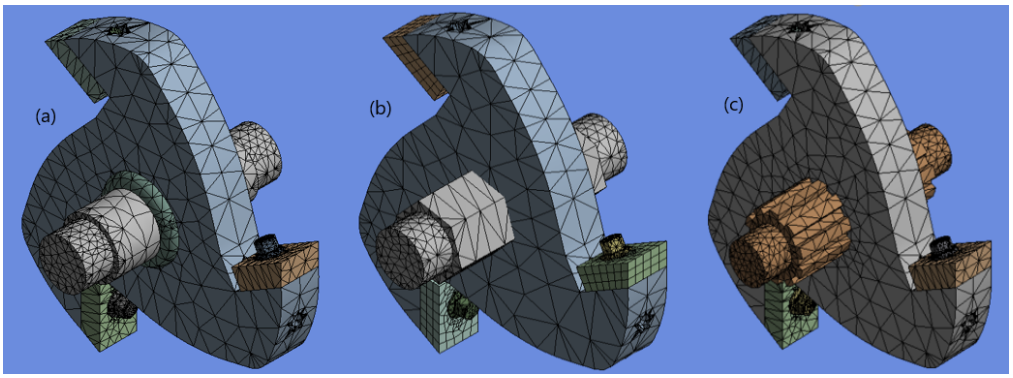


Figure 3: Finite element meshes: (a) cylindrical, (b) hexagonal, and (c) splined.

the parametric optimization model was meshed separately at 2 mm. Figure 3 displays the preliminary meshes.

The same loading and support arrangement was applied to each attachment configuration (Figure 4). A distributed line load of $q = 35.535$ N/mm was applied along the indicated blade-loading edge (label A), and fixed support conditions were imposed at the shaft support regions marked B. The resultant force associated with this edge load is $F = qL_{\text{load}}$, where L_{load} is the loaded edge length.

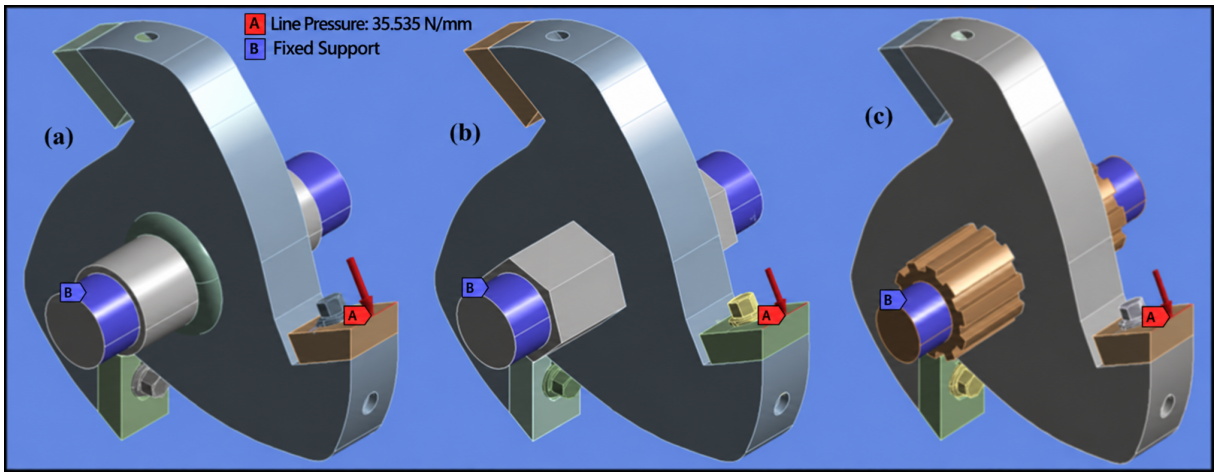


Figure 4: Load and support conditions: (a) cylindrical, (b) hexagonal, and (c) splined. A indicates the line load; B indicates the fixed support.

The splined arrangement was selected for the subsequent parametric study using the deformation and equivalent-stress responses from the preliminary attachment comparison, as discussed in Section 3.1. The selected blade carriage was parameterized in SolidWorks and imported into ANSYS Static Structural. The carriage material was modeled as structural steel using representative ASTM A36 properties, including a yield strength of $\sigma_y = 250$ MPa. The material constants are summarized in Table 1.

The parametric carriage model was discretized in ANSYS Mechanical using a target element size of $h = 2$ mm. The smallest nominal feature dimension was the 10 mm spline-way thickness (P_1), giving $h/P_1 = 0.20$, equivalent to five nominal element lengths across this feature. Since

Table 1: Material properties of ASTM A36.

Material property	Value	Unit
Young's modulus	200	GPa
Poisson's ratio	0.26	–
Shear modulus	79.37	GPa
Bulk modulus	138.89	GPa
Density	7850	kg/m^3
Yield strength	250	MPa
Ultimate tensile strength	400–550	MPa

P_1 varied from 9 to 11 mm during the DOE, the corresponding ratio ranged from 0.182 to 0.222. This discretization follows practical guidance on multiple elements through bending-dominated thicknesses and finer resolution in regions with high stress gradients [18, 19]. A mesh-convergence study was not performed; therefore, mesh independence of the predicted deformation and peak stress was not established.

A uniform pressure of 10 MPa was applied to the blade-retainer loading face, while a fixed support was prescribed on the internal splined interface, as illustrated in Figure 5. The structural responses extracted from ANSYS were maximum total deformation, maximum equivalent (von Mises) stress, and minimum yield-based factor of safety. For the von Mises yield criterion, the minimum safety factor was evaluated from

$$\mathrm{FoS}_{\min} = \frac{\sigma_y}{\sigma_{\mathrm{vM,max}}},$$

where σ_y is the assigned yield strength and $\sigma_{\mathrm{vM,max}}$ is the maximum equivalent stress.

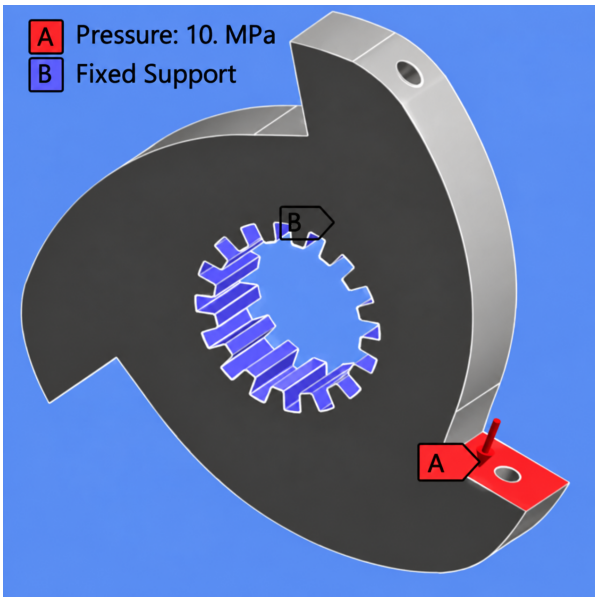


Figure 5: Load and boundary condition of the splined blade carriage: (A) 10 MPa pressure at the blade-retainer face and (B) fixed support at the internal splined interface.

2.2 Parametric Optimization

Five geometric features of the splined blade carriage were selected as design variables: spline-way thickness (P_1), outer radius of the spline (P_2), back blade retainer (P_4), corner fillet radius (P_5), and back radius of the carriage (P_6), as shown in Figure 6. Their initial dimensions were 10, 50, 30, 50, and 150 mm, respectively. The specified geometric limits are summarized in Table 2. Four parameters were assigned variations of ±10% around their initial values, whereas the back blade retainer (P_4) was assigned a wider interval of 23–37 mm.

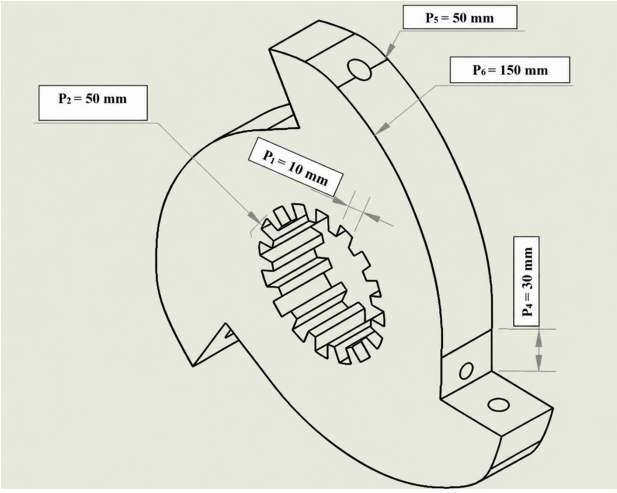


Figure 6: Parameterized geometric dimensions of the splined blade carriage.

Table 2: Initial geometric parameters and specified parameter bounds (mm).

Parameter	Feature	Initial	Lower	Upper
P_1	Thickness of spline way	10	9	11
P_2	Outer radius of spline	50	45	55
P_4	Back blade retainer	30	23	37
P_5	Corner fillet radius	50	45	55
P_6	Back radius of carriage	150	135	165

The structural output parameters were maximum total deformation (P_7), maximum equivalent stress (P_8), and minimum factor of safety (P_9). Figure 7 records the initial input values and the corresponding baseline outputs from the ANSYS parameter set; Figure 8 shows the interconnected structural analysis and Design Exploration systems.

Outline of All Parameters

	A	B	C	D
1	ID	Parameter Name	Value	Unit
2	Input Parameters			
3	Static Structural (A1)			
4	P1	Thickness of spline way	10	
5	P2	Outer radius of spline	50	
6	P4	Back blade retainer	30	
7	P5	Corner fillet radius	50	
8	P6	Back radius of carriage	150	
*	New input parameter	New name	New expression	
10	Output Parameters			
11	Static Structural (A1)			
12	P7	Total Deformation Maximum	0.07989	mm
13	P8	Equivalent Stress Maximum	155.52	MPa
14	P9	Safety Factor Minimum	1.6075	
*	New output parameter		New expression	
16	Charts			

Figure 7: Initial geometric input parameters and static structural output parameters in ANSYS Workbench.

The five-dimensional design space was sampled using a central composite design (CCD) in ANSYS DesignXplorer. The DOE comprised 27 design points: 16 fractional-factorial points, 10 axial points, and one center point [17]. For each design point, the geometry was updated and a static structural solution provided the three responses. The 27 design points provided the learning data for constructing the response surfaces.

The response surfaces were generated using the Genetic Aggregation method in ANSYS DesignXplorer. This approach combines candidate surrogate modelling techniques through an adaptive model-selection and aggregation procedure. Consequently, a single fixed polynomial order or prescribed set of interaction terms was not imposed on the final aggregated response models. The stored configuration specified a maximum of 12 genetic generations and manual refinement without additional refinement points. Separate response approximations were generated for deformation, equivalent stress, and factor of safety.

The response surfaces were examined using parameter-interaction plots and local and global sensitivity analyses. The agreement between surrogate predictions and finite element responses was assessed using the predicted-versus-observed data at the DOE learning points. The resulting surrogate models supplied the structural response evaluations used by the optimization algorithm.

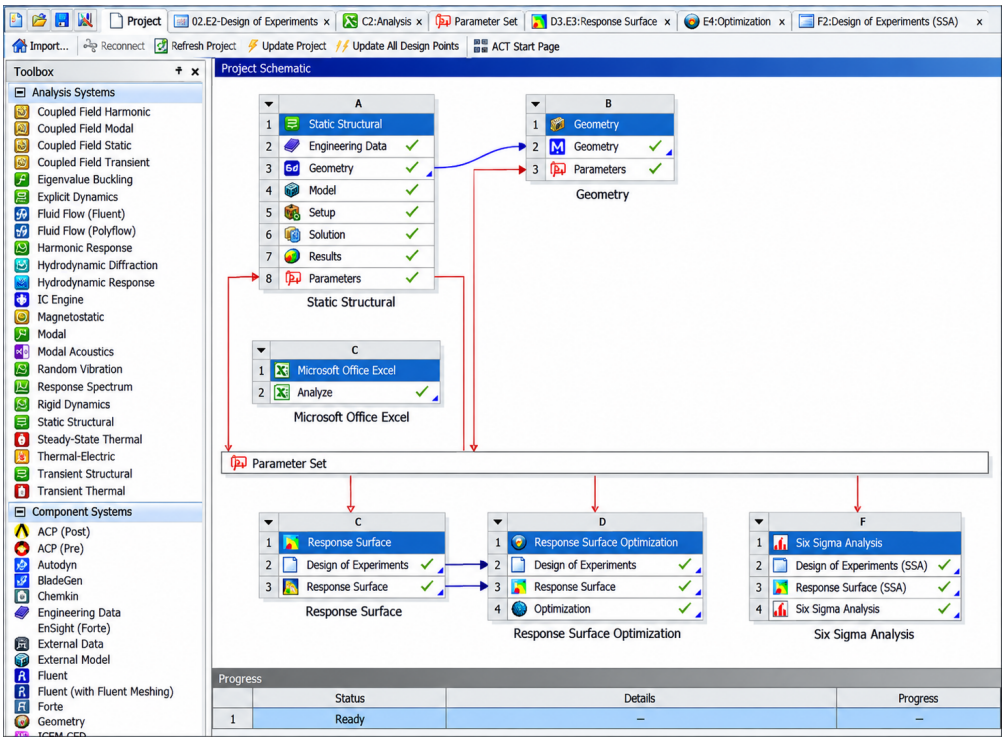


Figure 8: ANSYS Workbench arrangement for parametric analysis and optimization.

Multi-objective optimization was carried out using the Multi-Objective Genetic Algorithm (MOGA) within ANSYS DesignXplorer. The design vector is $\mathbf{p} = [P_1, P_2, P_4, P_5, P_6]^T$, and the optimization objectives were to minimize maximum deformation and equivalent stress while maximizing minimum factor of safety:

$$\begin{aligned} &\underset{\mathbf{p}}{\text{minimize}} \quad \big(P_7(\mathbf{p}), P_8(\mathbf{p}), -P_9(\mathbf{p})\big), \\ &\text{subject to} \quad \mathbf{p}_{\min} \le \mathbf{p} \le \mathbf{p}_{\max}. \end{aligned} \tag{1}$$

The algorithm returned three candidate solutions. These were compared using predicted deformation, equivalent stress, factor of safety, and the practicality of reconstructing the candidate dimensions in CAD. The response-surface predictions and selected final geometry are presented in Section 3.

3 Optimization Results and Discussion

3.1 Finite Element Analysis Results

The preliminary finite element analysis compared cylindrical, hexagonal, and splined shaft–carriage attachments. Figure 9 and Table 3 present the corresponding deformation contours and structural responses. The splined configuration exhibited the lowest maximum deformation (0.0283 mm) and equivalent von Mises stress (45.479 MPa), and was therefore selected for subsequent parametric optimization. The attachment comparison and parameterized carriage analysis were conducted using distinct finite element models.

The initial static structural analysis of the parameterized splined carriage was performed before parametric optimization. As shown in Figure 10, the maximum total deformation was 0.07989 mm, occurring at the outer blade-retaining regions, while the maximum equivalent

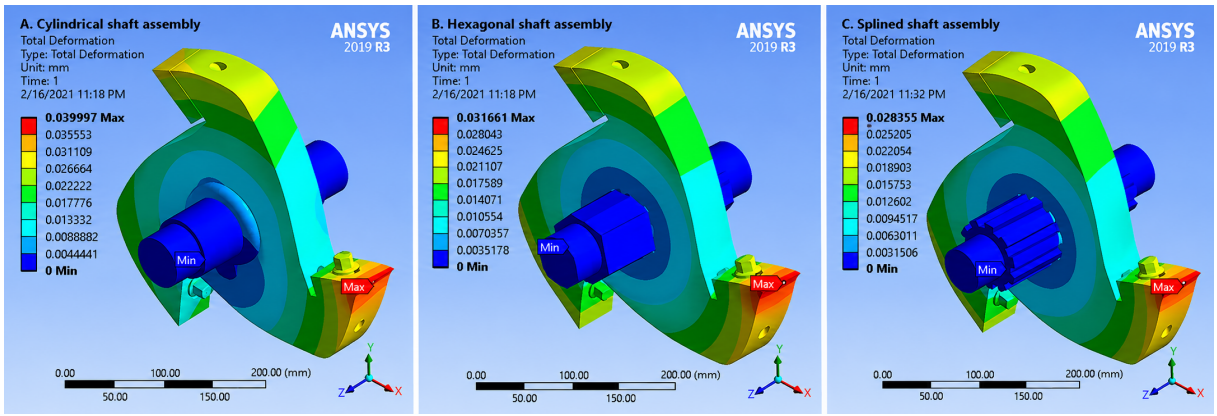
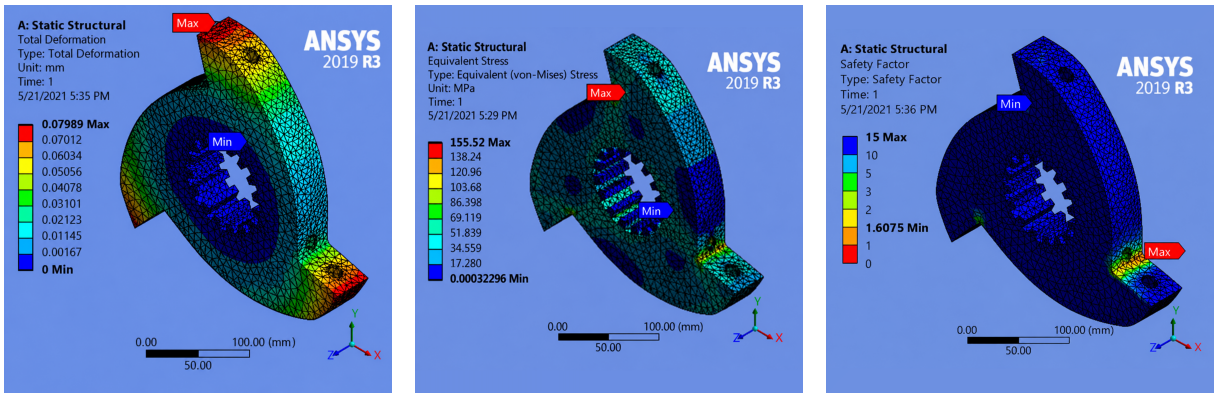


Figure 9: Total deformation contours for the three shaft–carriage attachment mechanisms.

Table 3: Comparative structural results for the shaft–carriage attachment mechanisms.

Attachment mechanism	Maximum deformation (mm)	Maximum von Mises stress (MPa)
Cylindrical	0.0399	216.92
Hexagonal	0.0316	45.483
Splined	0.0283	45.479

von Mises stress reached 155.52 MPa. The minimum factor of safety was 1.6075, consistent with the specified material yield strength of 250 MPa. Although the initial design satisfied the adopted static yield criterion, these results established the baseline for evaluating the subsequent parametric optimization.



(a) Total deformation (b) Equivalent stress (c) Factor of safety

Figure 10: Initial static structural analysis results of the splined blade carriage before parametric optimization.

3.2 Response surface and sensitivity analysis

The 27 DOE simulations characterized the influence of changes in carriage dimensions on deformation, equivalent stress, and factor of safety. The corresponding response trends are illustrated in Figures 11 and 12. In the reported design-point results, the largest and smallest deformations

occurred at design points 4 and 5, respectively; the highest and lowest equivalent stresses occurred at design points 2 and 3, respectively. The safety-factor trend was reversed for the latter two points, with the greatest factor of safety at design point 3.

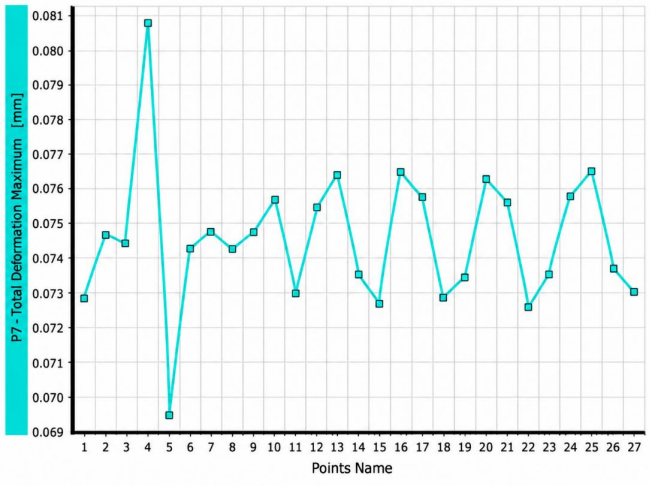


Figure 11: Maximum deformation obtained at the DOE design points.

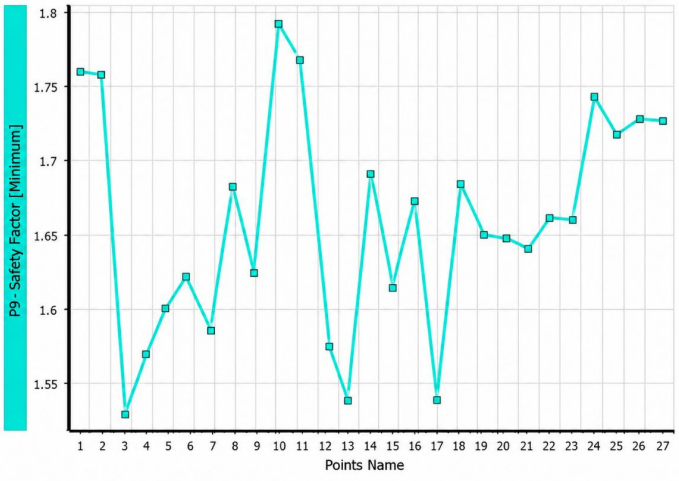
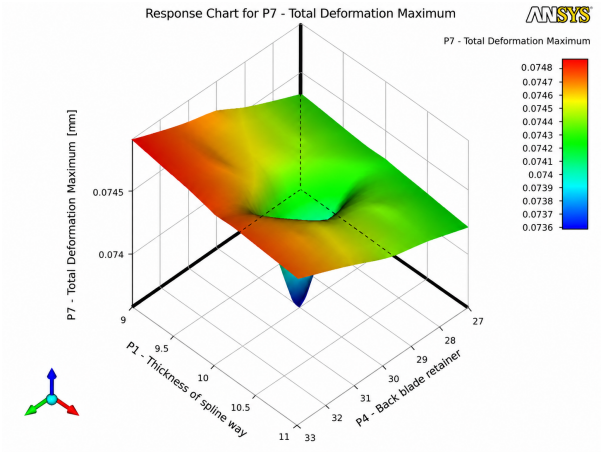


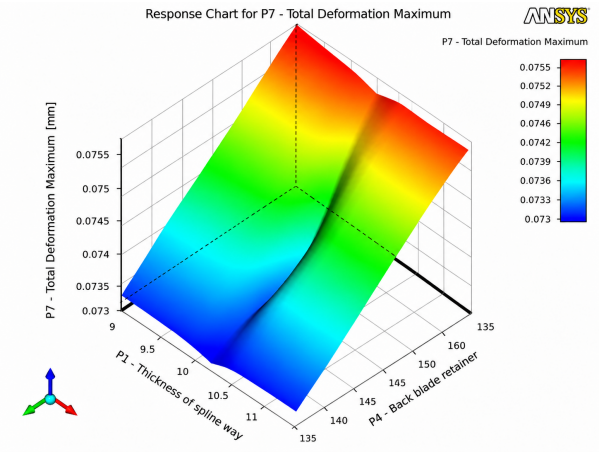
Figure 12: Minimum factor of safety obtained at the DOE design points.

The response surfaces provide continuous approximations of the structural responses over the sampled design space. Figure 13 presents selected two-parameter views: P_1 and P_4 versus deformation, P_1 and P_6 versus deformation, P_1 and P_6 versus equivalent stress, and P_2 and P_6 versus minimum factor of safety. These plots illustrate that the structural responses are sensitive to coupled changes in carriage geometry rather than to a single dimension alone.

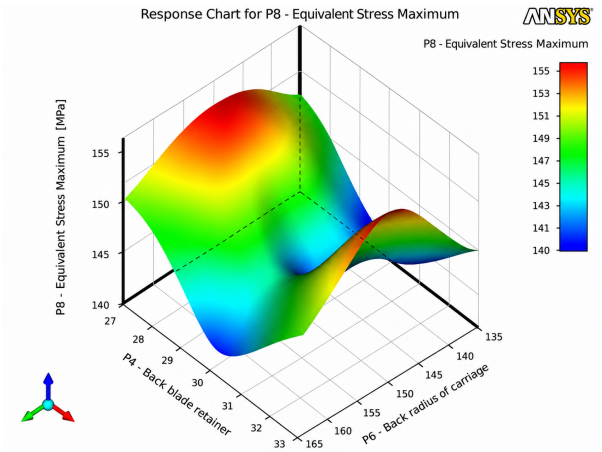
Local sensitivity curves were used to assess the effect of each geometric parameter on a structural response while holding the remaining parameters at their reference settings. Figure 14 shows the trends for deformation; Figures 15 and 16 show the corresponding trends for equivalent stress and safety factor. The reported sensitivity plots indicate that the spline-way thickness (P_1) has an important influence on equivalent stress and minimum safety factor,



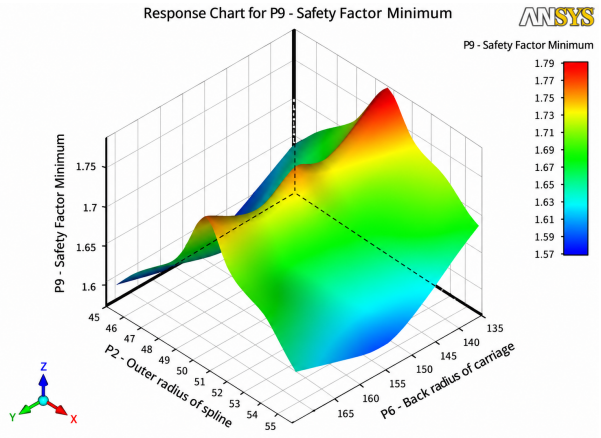
(a) P_1 and P_4 versus P_7



(b) P_1 and P_6 versus P_7



(c) P_1 and P_6 versus P_8



(d) P_2 and P_6 versus P_9

Figure 13: Selected response surfaces for total deformation (P_7), equivalent stress (P_8), and minimum factor of safety (P_9).

whereas radius parameters also affect deformation. Global sensitivities (Figure 17) summarize parameter influence over the design space and complement the local curves.

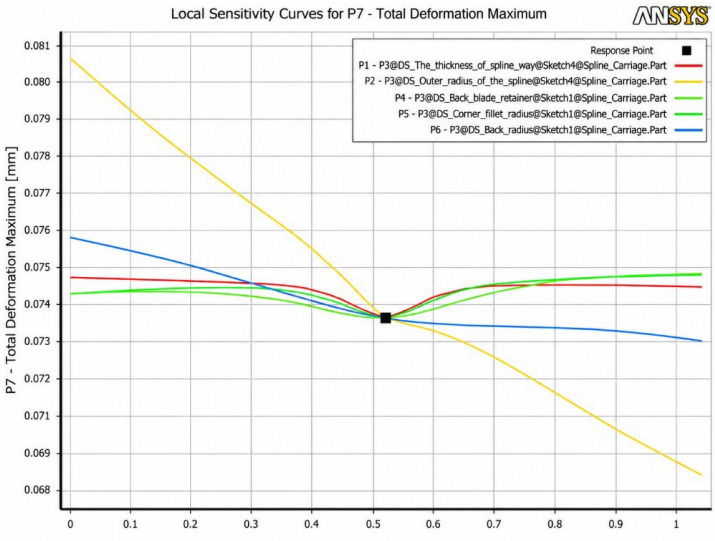


Figure 14: Local sensitivity curves for maximum deformation.

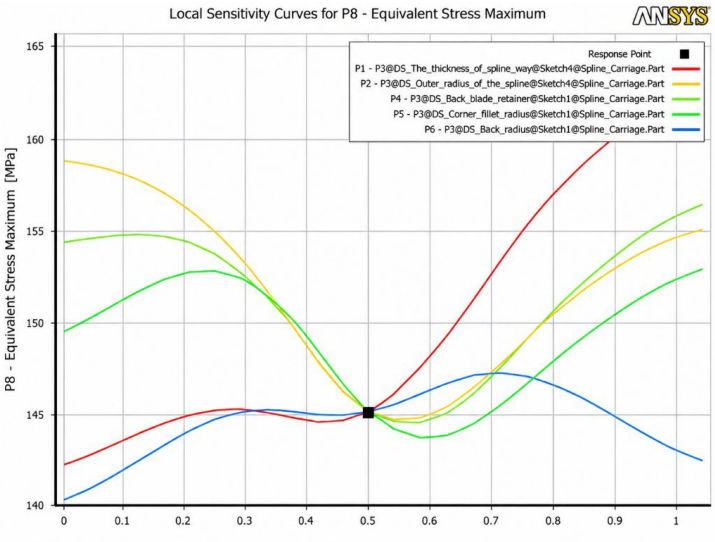


Figure 15: Local sensitivity curves for maximum equivalent stress.

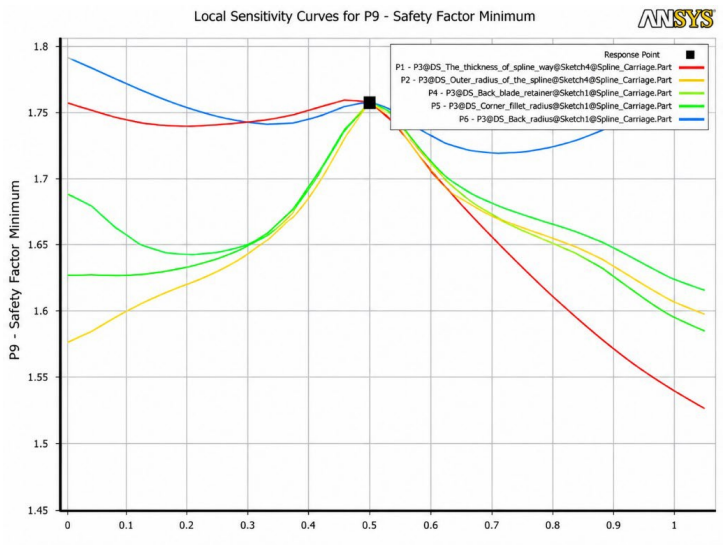


Figure 16: Local sensitivity curves for minimum factor of safety.

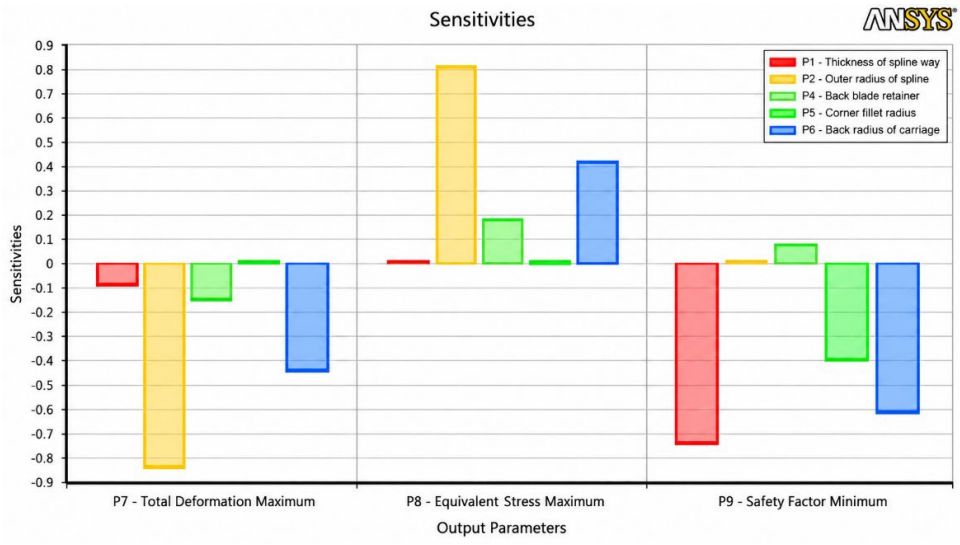


Figure 17: Global sensitivities of structural responses to the geometric input parameters.

The agreement between the response-surface predictions and the corresponding FEA responses was evaluated using the coefficient of determination (R^2) and root mean square error (RMSE). For n observations, the goodness-of-fit measures were defined as

$$R^2 = 1 - \frac{\sum_{i=1}^{n}(y_i - \widehat{y}_i)^2}{\sum_{i=1}^{n}(y_i - \overline{y})^2}, \qquad \mathrm{RMSE} = \sqrt{\frac{1}{n}\sum_{i=1}^{n}(y_i - \widehat{y}_i)^2}. \tag{2}$$

Here, y_i is the FEA response, $\widehat{y}_i$ is the corresponding surrogate prediction, $\overline{y}$ is the mean of the FEA responses, and n is the number of evaluated design points. The goodness-of-fit indices were calculated using the 27 learning-point pairs stored in the ANSYS response-surface project.

Table 4 summarizes the calculated goodness-of-fit indices. The coefficients of determination were 0.993907 for deformation, 0.970627 for equivalent stress, and approximately 1.000000 for minimum factor of safety. The corresponding RMSE values were 1.5564×10^{-4} mm, 1.15524 MPa, and 3.39×10^{-9}, respectively. These values indicate close agreement between the surrogate predictions and the FEA results at the learning points. The reported metrics measure in-sample fitting accuracy and do not establish independent predictive accuracy.

Table 4: Training-point goodness-of-fit indices calculated from the 27-point ANSYS DOE.

Structural response	R^2	RMSE
Maximum deformation (P_7)	0.993907	1.5564×10^{-4} mm
Maximum equivalent stress (P_8)	0.970627	1.15524 MPa
Minimum factor of safety (P_9)	≈ 1.000000	3.39×10^{-9}

Figure 18 compares the response-surface predictions with the corresponding FEA responses. The diagonal reference line represents perfect agreement, while deviations from this line represent prediction residuals at the evaluated learning points.

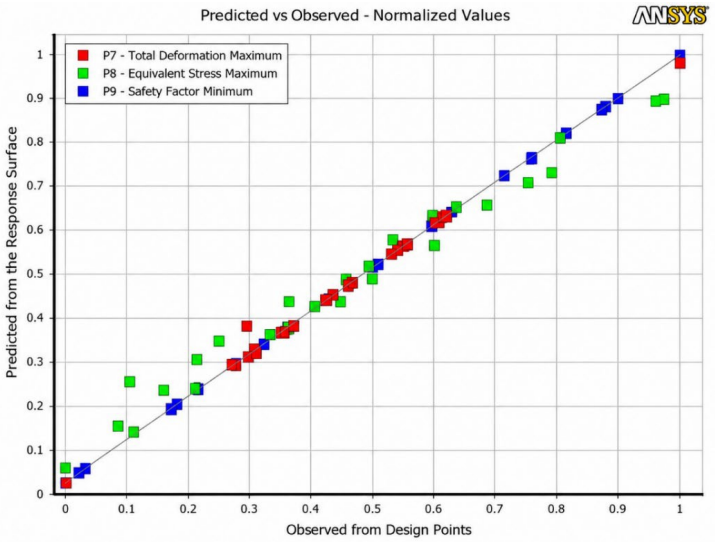


Figure 18: Predicted-versus-observed goodness-of-fit chart for the response-surface models.

3.3 Optimal design selection and performance assessment

The MOGA-based response-surface optimization generated three candidate solutions, shown in Figure 19 and summarized in Table 5. The optimization exposes a trade-off among objectives: Candidate 3 has the smallest reported predicted deformation (0.071006 mm), whereas Candidate 1 has the lowest tabulated predicted stress (143.08 MPa) and the highest tabulated predicted safety factor (1.7808) among the three solutions. Thus, Candidate 3 is not uniformly best across all objectives; it represents a selection emphasizing deformation and a geometry judged suitable for further detailing.

Table of Schematic E4 Optimization				
	A	B	C	D
1	Optimization Study			
2	Minimize P7; P7 >= 0.071 mm	Goal, Minimize P7 (Default importance); Strict Constraint, P7 values greater than or equals to 0.071 mm (Default importance)		
3	Minimize P8; P8 >= 141 MPa	Goal, Minimize P8 (Default importance); Strict Constraint, P8 values greater than or equals to 141 MPa (Default importance)		
4	Maximize P9; P9 <= 1.8	Goal, Maximize P9 (Default importance); Strict Constraint, P9 values less than or equals to 1.8 (Default importance)		
5	Optimization Method			
6	MOGA	The MOGA method (Multi-Objective Genetic Algorithm) is a variant of the popular NSGA-II (Non-dominated Sorted Genetic Algorithm-II) based on controlled elitism concepts. It supports multiple objectives and constraints and aims at finding the global optimum.		
7	Configuration	Generate 5000 samples initially, 1000 samples per iteration and find 3 candidates in a maximum of 20 iterations.		
8	Status	Converged after 10724 evaluations.		
9	Candidate Parts			
10		Candidate Point 1	Candidate Point 2	Candidate Point 3
11	P1 - Thickness of spline way	9.0191	9.0191	9.0292
12	P2 - Outer radius of spline	54.468	54.469	52.365
13	P4 - Back blade retainer	30.56	36.727	36.717
14	P5 - Corner fillet radius	47.993	50.683	50.838
15	P6 - Back radius of carriage	135.34	136.3	162.53
16	P7 - Total Deformation Maximum (mm)	0.071104	0.071121	0.071006
17	P8 - Equivalent Stress Maximum (MPa)	143.08	143.12	143.35
18	P9 - Safety Factor Minimum	1.7996	1.7922	1.7586

Figure 19: Response-surface optimization and candidate design selection.

Table 5: MOGA candidate geometries and response-surface-predicted structural outputs.

Candidate	Design parameters (mm)					Predicted responses		
	P_1	P_2	P_4	P_5	P_6	Deformation (mm)	Stress (MPa)	Minimum FoS
1	9.02	54.47	30.56	47.54	135.34	0.071107	143.08	1.7808
2	9.02	54.47	30.73	50.68	136.30	0.071121	143.12	1.7786
3	9.03	52.36	30.72	50.84	162.53	0.071006	143.35	1.7692

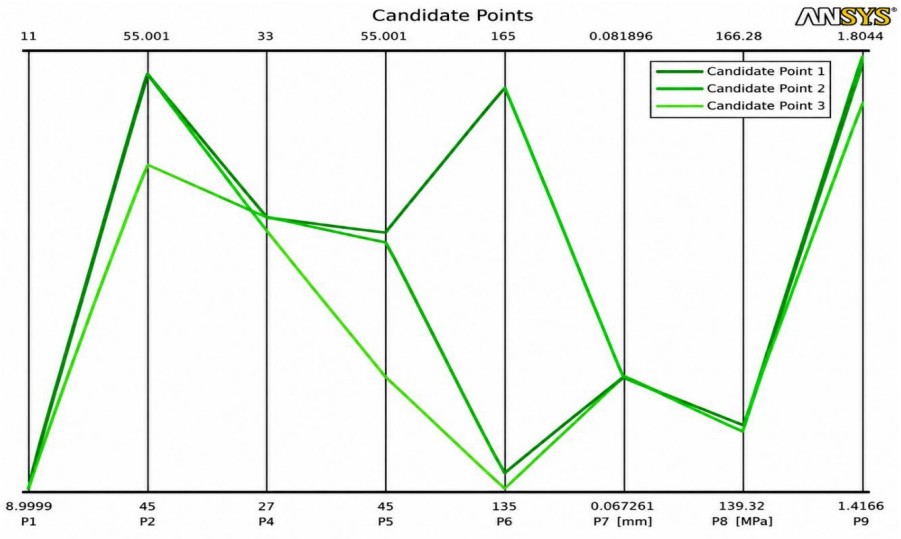


Figure 20: Comparison of the candidate design points.

The dimensions of Candidate 3 were rounded to nominal values for the reconstructed CAD geometry, namely $P_1 = 9$, $P_2 = 52.5$, $P_4 = 31$, $P_5 = 51$, and $P_6 = 162.5$ mm. The dimensional

rounding produces a more concise geometric specification; the unrounded optimized values remain reported in Table 5.

Table 6 compares the original FEA responses obtained at the initial parameters (Figure 7) with the reported surrogate predictions of Candidate 3. Reductions in deformation and stress were calculated using

$$\Delta_y(\%) = \frac{y_{\text{original}} - y_{\text{candidate}}}{y_{\text{original}}} \times 100. \tag{3}$$

The percentage increase in minimum factor of safety was calculated using

$$\Delta_{\text{FoS}}(\%) = \frac{\text{FoS}_{\text{candidate}} - \text{FoS}_{\text{original}}}{\text{FoS}_{\text{original}}} \times 100. \tag{4}$$

Based on the tabulated surrogate predictions, the numerical comparison indicates an 11.12% reduction in maximum deformation, a 7.83% reduction in maximum equivalent stress, and a 10.06% increase in minimum factor of safety. These values describe the predicted response differences between the original design and unrounded Candidate 3, rather than independently verified improvements for the reconstructed final geometry.

Table 6: Original FEA design versus response-surface-predicted Candidate 3.

Performance measure	Original FEA	Candidate 3 (predicted)	Change (%)
Maximum deformation (mm)	0.079890	0.071006	−11.12
Maximum equivalent stress (MPa)	155.52	143.35	−7.83
Minimum factor of safety	1.6075	1.7692	+10.06

Figure 21 shows the reconstructed blade carriage with the selected nominal dimensions. The performance figures in Table 6 correspond to the unrounded surrogate candidate rather than a direct static structural reanalysis of the rounded CAD model. The reconstruction therefore establishes the selected dimensional configuration, while its final structural response remains distinct from the surrogate-predicted candidate response.

4 Conclusions

A response-surface-based parametric optimization study of a splined plastic-shredder rotor blade carriage was conducted using SolidWorks and ANSYS Workbench. Five geometric parameters were investigated using a 27-point central composite design, and surrogate models were constructed using the Genetic Aggregation approach. The multi-objective genetic algorithm produced three candidate designs evaluated in terms of maximum deformation, maximum equivalent stress, and minimum factor of safety.

The training-point goodness-of-fit analysis gave coefficients of determination of 0.9939, 0.9706, and approximately 1.0000 for deformation, equivalent stress, and factor of safety, respectively. The corresponding RMSE values were 1.5564×10^{-4} mm, 1.1552 MPa, and 3.39×10^{-9}. These measures indicate good agreement between the surrogate models and the sampled finite element responses, without establishing independent predictive accuracy.

Candidate 3 was selected for CAD reconstruction because it provided the smallest tabulated predicted deformation among the three reported candidates. Relative to the original FEA results, its unrounded response-surface predictions indicate an 11.12% reduction in deformation, a

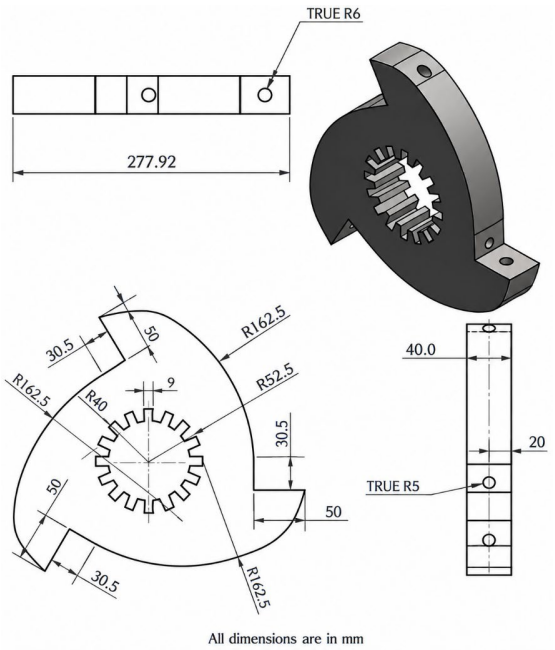


Figure 21: Reconstructed splined blade carriage after parametric optimization.

7.83% reduction in equivalent stress, and a 10.06% increase in minimum factor of safety. These improvements remain surrogate-based estimates rather than direct finite element results for the final rounded CAD geometry. The numerical assessment is further limited by the absence of a mesh-convergence study and independent response-surface validation. Future work should examine fatigue life, modal behavior, and the manufacturing tolerances of the reconstructed carriage.

Acknowledgements
The authors gratefully acknowledge Mizan-Tepi University for funding this research.

References

[1] Ragaert K, Delva L and Van Geem K 2017 Mechanical and chemical recycling of solid plastic waste. *Waste Manage.*, 69, 24–58, doi: 10.1016/j.wasman.2017.07.044.

[2] Uzosike C C, Yee L H and Padilla R V 2023 Small-scale mechanical recycling of solid thermoplastic wastes: A review of PET, PEs, and PP. *Energies (Basel)*, 16(3), 1406, doi: 10.3390/en16031406.

[3] Wong J H, Gan M J H, Chua B L, Gakim M and Siambun N J 2022 Shredder machine for plastic recycling: A review paper. *IOP Conf. Ser.: Mater. Sci. Eng.*, 1217(1), 012007, doi: 10.1088/1757-899X/1217/1/012007.

[4] Tyflopoulos E and Steinert M 2020 Topology and parametric optimization-based design processes for lightweight structures. *Appl. Sci.*, 10(13), 4496, doi: 10.3390/app10134496.

[5] Tang P-S and Chang K-H 2001 Integration of topology and shape optimization for design of structural components. *Struct. Multidiscip. Optim.*, 22(1), 65–82, doi: 10.1007/PL00013282.

[6] Park H-S and Dang X-P 2010 Structural optimization based on CAD–CAE integration and metamodeling techniques. *Comput.-Aided Des.*, 42(10), 889–902, doi: 10.1016/j.cad.2010.06.003.

[7] Jin R, Chen W and Simpson T W 2001 Comparative studies of metamodelling techniques under multiple modelling criteria. *Struct. Multidiscip. Optim.*, 23(1), 1–13, doi: 10.1007/s00158-001-0160-4.

[8] Box G E P and Wilson K B 1951 On the experimental attainment of optimum conditions. *J. R. Stat. Soc. Ser. B*, 13(1), 1–38, doi: 10.1111/j.2517-6161.1951.tb00067.x.

[9] Montgomery D C 2017 *Design and Analysis of Experiments*, 9th ed. Wiley.

[10] Cavazzuti M, Baldini A, Bertocchi E, Costi D, Torricelli E and Moruzzi P 2011 High performance automotive chassis design: A topology optimization-based approach. *Struct. Multidiscip. Optim.*, 44(1), 45–56, doi: 10.1007/s00158-010-0578-7.

[11] Li C, Kim I Y and Jeswiet J 2015 Conceptual and detailed design of an automotive engine cradle by using topology, shape, and size optimization. *Struct. Multidiscip. Optim.*, 51(2), 547–564, doi: 10.1007/s00158-014-1151-6.

[12] Zhu J-H, Zhang W-H and Xia L 2016 Topology optimization in aircraft and aerospace structures design. *Arch. Comput. Methods Eng.*, 23(4), 595–622, doi: 10.1007/s11831-015-9151-2.

[13] Kefyalew E, Fikadu A and Gopal M 2026 Parametric topology optimization of a cylinder mounting bracket using PTC Creo. *ITEGAM-JETIA*, 12(60), 1523–1535, doi: 10.5935/jetia.v12i60.4433.

[14] Trad A, Amoura N, Abdellah El-Hadj A and Kebir H 2024 Optimizing plastic shredder rotor design through structural finite element analysis: A comprehensive approach using experimental design and response surface methodology. *Mech. Based Des. Struct. Mach.*, 52(12), 10682–10701, doi: 10.1080/15397734.2024.2360680.

[15] Tesema E K and Lemu H G 2024 Topology optimization of plastic shredding machine blade carriage. Advanced Manufacturing and Automation XIII, Lecture Notes in Electrical Engineering, 1154, 687–694, doi: 10.1007/978-981-97-0665-5_84.

[16] Nguyen T K, Chau M Q, Do T-C and Pham A-D 2021 Characterization of geometrical parameters of plastic bottle shredder blade utilizing a two-step optimization method. *Arch. Mech. Eng.*, 68(3), 253–269, doi: 10.24425/ame.2021.138392.

[17] ANSYS, Inc. 2025 *DesignXplorer User's Guide*, Release 2025 R2. Available at: https://ansyshelp.ansys.com/public/Views/Secured/corp/v252/en/pdf/DesignXplorer_Users_Guide.pdf.

[18] Autodesk, Inc. n.d. *Mesh quality*. Autodesk Fusion Simulation Help. Available at: https://help.autodesk.com/cloudhelp/ENU/Fusion-Simulate/files/SIM-MESH-QUALITY.htm.

[19] ANSYS, Inc. 2025 *Mesh Quality Best Practices*. ANSYS Discovery User Manual, Release 2025 R2. Available at: https://ansyshelp.ansys.com/public/Views/Secured/corp/v252/en/discovery/UDA/user_manual/meshing/topics/r_meshquality_bestpractices.html.